Reply to "Comment on 'Bottom-Up Graphene-Nanoribbon Fabrication Reveals Chiral Edges and Enantioselectivity'"

■ Simonov *et al.* have used a combination of surface-science techniques, including room-temperature (RT) scanning tunneling microscopy (STM), to investigate 10,10′-dibromo-9,9′-bianthryl (DBPM), a precursor monomer of graphene nanoribbons (GNRs), on Cu{111} at high DBPM coverage and slow sample annealing speeds.[1,2] They found that the product is a seven-carbon-wide armchair graphene nanoribbon (7-AGNR), as previously observed on Au{111} and Ag{111}.[3,4] In our recent article, we used low-temperature (LT) STM to probe DBPM/Cu{111} at low DBPM coverage and fast annealing speeds.[5] We found that the product is the (3,1)-chiral-edge GNR ((3,1)-GNR). As described in this Reply, we fabricated GNRs by annealing DBPM/Cu{111} under kinetic conditions close to those in ref 2. Using LT STM, we resolved the atomic structure of the product GNRs. We demonstrate that the GNRs investigated by refs 2 and 5 are likely to be the same structure.

Imaging Graphene Nanoribbons Fabricated under the Same Kinetic Conditions as Simonov *et al.* In their Comment, Simonov *et al.* propose that DBPM polymerization on Cu{111} may be kinetically controlled to yield GNRs of different edge configurations, *via* different mechanisms.[1] Specifically, for higher coverage DBPM/Cu{111}, a slow annealing rate would successively trigger debromination, polymerization, and cyclodehydrogenation (CDH), forming 7-AGNR (Scheme 1 in Figure 1; *i.e.*, *via* the Ullmann coupling reaction[3]); for lower coverage DBPM/Cu{111}, a fast annealing rate would promote island formation followed by debromination and CDH, forming (3,1)-GNR (Scheme 2 in Figure 1).[5] To test this hypothesis, we use our results from ref 5, reproduced below (Figure 2a and blue line in 2c), as reference. We then perform a set of comparative experiments by depositing DBPM on clean Cu{111} at higher coverages, heating the sample at slower rates, and annealing the sample for longer times (Figure 2b and red line in 2c), thus emulating the experimental conditions of Simonov *et al.*

As our STM image in the top panel of Figure 2b indicates, the new fabrication conditions (which attempt to reproduce those from ref 2) yielded a GNR morphology closely resembling that shown in Figure 2e of ref 2. Moreover, our high-resolution STM images in Figure 2b, bottom panel, confirm that the "zigzag shape" of our GNR edges is caused by the atomic structure of the (3,1)-GNR. Therefore, we conclude that, as of yet, we find no STM evidence that the polymerization of DBPM on Cu{111} can be kinetically controlled to select the edge conformation of the resulting GNRs. Instead, our current work supports our original conclusion in ref 5 that DBPM polymerization on Cu{111} produces (3,1)-GNRs due to the substrate's surface atomic structure and catalytic properties (Scheme 2). The fact that our newest results *still* show the formation of (3,1)-GNRs under conditions close to ref 2

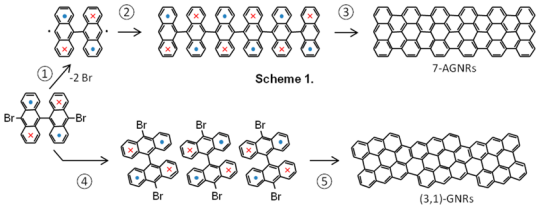

Figure 1. Two proposed mechanisms for 10,10′-dibromo-9,9′-bianthryl alignment on Cu{111}. The circled numbers denotes individual mechanistic steps. ① Surface-catalyzed debromination. ② Polymerization. ③ Cyclodehydrogenation (CDH). ④ Molecular alignment. ⑤ Debromination and CDH.

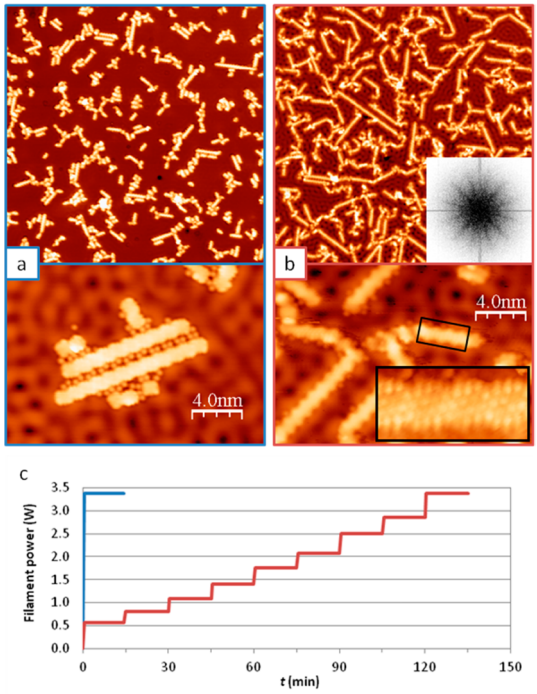

Figure 2. Effects of 10,10′-dibromo-9,9′-bianthryl coverage, sample heating speeds, and sample annealing times. (a) Topographic STM images from ref 5 showing (3,1)-GNRs (top panel, 100 nm × 100 nm; bottom panel, 20 nm × 14 nm). The sample heating speed and annealing time used to obtain (a) are shown as the blue line in (c). (b) Topographic STM images (top panel, 100 nm × 100 nm; bottom panel, 20 nm × 14 nm) showing (3,1)-GNRs fabricated at higher DBPM coverage, slower sample heating rate, and longer sample annealing time with respect to (a). The sample heating speed and annealing time used to obtain (b) are shown as the red line in (c). The top panel inset of (b) shows the two-dimensional Fourier transform image of the main panel. The bottom panel inset of (b) shows the atomically resolved STM image of the location indicated by the black rectangles. In this latter image, only α-carbons are observed as circular protrusions. (c) Sample heating speeds and annealing rates used to obtain (a) and (b) in terms of power supplied to the heating filament. A filament power of 3.4 W corresponds to ~500 °C (refer to Figure 3 for the relationship between the substrate temperature and the filament power).

precludes the mechanism in Scheme 1 because the polymer structure resulting from ② cannot form the chiral-edge nanoribbons without substantial rearrangement of C−C bonds. We have not observed 7-AGNR postulated by Simonov *et al.*;[1] thus, we refrain from speculating further on their data interpretation and hypotheses.

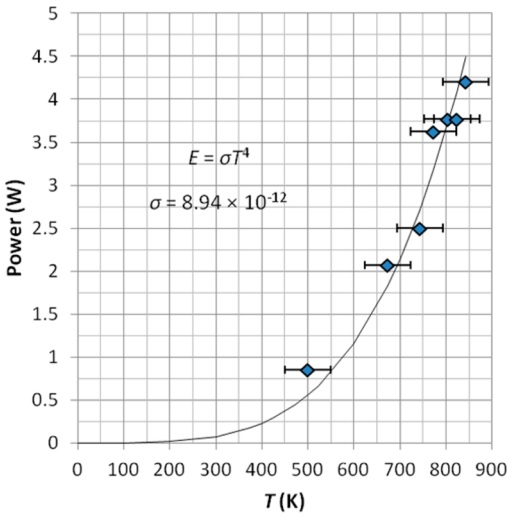

Figure 3. Measured sample temperature *versus* supplied filament power. Blue squares show the temperature of the Cu{111} surface during annealing with the corresponding power supplied to the heating filament. The curve shows the T^4 function fitted for $T > 600$ K according to the Stefan–Boltzmann law.

A Note on Measuring Annealing Temperature. Simonov *et al.* point out that the temperatures we reported in ref 5 seem high compared to theirs, and that it is difficult to compare each of our STM images of surfaces subjected to different annealing conditions. For example, while Figure 3 from ref 1 shows GNRs decomposed after a 15 min sample anneal at 450 °C, our Figure 3 in ref 5 shows defect-free (3,1)-GNRs formed after a 10 min sample anneal at 500 °C.

Here, we note that our experimental requirements limit the accuracy of infrared pyrometry. We are most interested in temperatures ranging from RT to 500 °C; on the other hand, we anneal our small Cu sample, a low-emissivity material, using a filament as radiant heat source, located—from the pyrometer's viewpoint—behind the crystal. During annealing, the light emitted by the filament is visible with the naked eye. Therefore, it is conceivable that during temperature measurements, even though the focus spot size covers the Cu surface exclusively, stray radiation from the filament is still detected. These conditions may combine to produce measured temperatures systematically higher than the actual temperature. We use a model Impac IGA 8 pro pyrometer, LumaSense Technologies, set to 10% emissivity when probing Cu{111}, with a focal spot size of 1 mm. The Cu sample size is 7.0 mm × 2.5 mm with a thickness of 0.6 mm. For completeness, we show the measured Stefan–Boltzmann relationship of our system in Figure 3. An emissivity of 0.1 was used for probing Cu{111} surface.

REFERENCES AND NOTES

1. Simonov, K. A.; Vinogradov, N. A.; Vinogradov, A. S.; Generalov, A. V.; Zagrebina, E. M.; Martensson, N.; Cafolla, A. A.; Carpy, T.; Cunniffe, J. P.; Preobrajenski, A. B. Comment on "Bottom-Up Graphene-Nanoribbon Fabrication Reveals Chiral Edges and Enantioselectivity". *ACS Nano* **2015**, 10.1021/nn506439a.
2. Simonov, K. A.; Vinogradov, N. A.; Vinogradov, A. S.; Generalov, A. V.; Zagrebina, E. M.; Martensson, N.; Cafolla, A. A.; Carpy, T.; Cunniffe, J. P.; Preobrajenski, A. B. Effect of Substrate Chemistry on the Bottom-Up Fabrication of Graphene Nanoribbons: Combined Core-Level Spectroscopy and STM Study. *J. Phys. Chem. C* **2014**, *118*, 12532–12540.
3. Cai, J.; Ruffieux, P.; Jaafar, R.; Bieri, M.; Braun, T.; Blankenburg, S.; Muoth, M.; Seitsonen, A. P.; Saleh, M.; Feng, X.; et al. Atomically Precise Bottom-Up Fabrication of Graphene Nanoribbons. *Nature* **2010**, *466*, 470–473.
4. Huang, H.; Wei, D.; Sun, J.; Wong, S. L.; Feng, Y. P.; Castro Neto, A. H.; Wee, A. T. S. Spatially Resolved Electronic Structures of Atomically Precise Armchair Graphene Nanoribbons. *Sci. Rep.* **2012**, *2*, 983.
5. Han, P.; Akagi, K.; Canova, F. F.; Mutoh, H.; Shiraki, S.; Iwaya, K.; Weiss, P. S.; Asao, N.; Hitosugi, T. Bottom-Up Graphene-Nanoribbon Fabrication Reveals Chiral Edges and Enantioselectivity. *ACS Nano* **2014**, *8*, 9181–9187.

Patrick Han,[*,†,‡] Kazuto Akagi,[†] Filippo Federici Canova,[†] Hirotaka Mutoh,[†] Susumu Shiraki,[†] Katsuya Iwaya,[§] Paul S. Weiss,[†,‡] Naoki Asao,[*,†] and Taro Hitosugi[†]

[†]Advanced Institute for Materials Research (AIMR), Tohoku University, Sendai 980-8577, Japan

[‡]California NanoSystems Institute and Departments of Chemistry and Biochemistry and Materials Science and Engineering, University of California, Los Angeles, Los Angeles, California 90095, United States

[§]RIKEN Center for Emergent Matter Science (CEMS), Wako, Saitama 351-0198, Japan

*Address correspondence to pxh@wpi-aimr.tohoku.ac.jp, asao@m.tohoku.ac.jp.

Received for review March 19, 2015

Published online April 28, 2015
10.1021/acsnano.5b01687